Active site assembly by SMG5 as a mechanism for SMG6 endonuclease licensing in nonsense-mediated mRNA decay

Enes S. Arpa[1*], Michael Taschner[2*], Mara De Matos[1], Stefanie Jonas[3#], David Gatfield[1#]

Affiliations:

[1] Center for Integrative Genomics (CIG), University of Lausanne, 1015 Lausanne, Switzerland.

[2] Department of Fundamental Microbiology (DMF), University of Lausanne, 1015 Lausanne, Switzerland.

[3] Department of Biology, Institute of Molecular Biology and Biophysics, ETH Zurich, 8093 Zurich, Switzerland.

[*] shared first authorship

[#] corresponding authors

e-mail addresses: enessalih.arpa@unil.ch, michael.taschner@unil.ch, mara.dematos@unil.ch, stefanie.jonas@mol.biol.ethz.ch, david.gatfield@unil.ch

Abstract

Nonsense-mediated mRNA decay (NMD) is a conserved eukaryotic surveillance pathway that eliminates transcripts containing premature termination codons (PTCs). While the recognition phase of NMD is well characterised, the effector step – how targeted mRNAs are nucleolytically degraded – remains incompletely understood. In metazoans, NMD employs an endonucleolytic route mediated by SMG6, a PIN-domain nuclease, alongside SMG5 and SMG7, which act downstream of PTC recognition. SMG5 has recently been proposed to license SMG6 activity, yet the molecular basis of this licensing has remained elusive. Here, we combine AlphaFold structural predictions with biochemical assays to investigate interactions among human SMG5, SMG6, and SMG7. Structural models predict a high-confidence interface between SMG5 and SMG6 PIN domains that forms a composite active site: a conserved SMG5 aspartate (D893) complements the SMG6 acidic triad to reinstate the canonical tetrad required for PIN-domain catalysis. *In vitro*, SMG6 alone exhibits weak endonucleolytic activity, which is enhanced ~10-fold by SMG5 PIN. Mutational analyses confirm that conserved residues from both proteins are essential for this composite configuration. Our findings reveal that the SMG5 PIN domain, previously considered catalytically inert, plays a critical role in activating SMG6 by completing its active site. This work provides mechanistic insight into the SMG5-dependent licensing step and uncovers a composite PIN nuclease architecture at the heart of the metazoan NMD effector phase.

Keywords: nonsense-mediated mRNA decay (NMD); PIN domain; UPF1 phosphorylation; endonucleolytic decay; SMG5-SMG6 interaction; RNA surveillance; in vitro nuclease assay

Introduction

Nonsense-mediated mRNA decay (NMD) was first recognized more than three decades ago as a conserved eukaryotic mRNA surveillance pathway that selectively degrades transcripts containing premature termination codons (PTCs) [1]. Early genetic screens in *Saccharomyces cerevisiae* [2] and *Caenorhabditis elegans* [3] identified the core Upf (up-frameshift) and Smg (suppressor of morphogenesis on genitalia) factors, defining a pathway that is conserved from yeast to humans. Subsequent work across species has established the “rules of NMD” – i.e., the molecular features that determine whether a terminating ribosome triggers or escapes NMD recognition and activation. By contrast, the effector phase – how targeted transcripts are ultimately degraded – took longer to resolve. NMD was long thought to rely primarily on accelerated general exonucleolytic mRNA turnover rather than specialized nucleases [4, 5]. It is now clear, however, that NMD recruits both exonucleolytic and endonucleolytic decay mechanisms, with striking mechanistic divergence between yeast and metazoans [6].

In yeast, NMD relies predominantly on the canonical decapping-dependent 5'→3' exonucleolytic decay pathway [7]. Once marked for NMD, transcripts are decapped by Dcp1/Dcp2 and rapidly degraded by the 5'→3' exonuclease Xrn1, with the 3'→5' exosome contributing to a lesser extent [4, 8]. This paradigm established NMD as a pathway that co-opts general mRNA decay machinery rather than deploying pathway-specific nucleases.

By contrast, the situation in metazoans is more complex. Two key discoveries reshaped current models: first, that NMD substrates in *Drosophila melanogaster* undergo endonucleolytic cleavage near the PTC [9], and second, that *Drosophila* and human SMG6 proteins harbour an active PIN (PilT N-terminal) endonuclease domain domain [10-12]. In the prevailing model, SMG6 – representing the first dedicated nuclease intrinsic to the NMD machinery – directly cleaves target mRNAs, generating unprotected 3' and 5' fragments that are subsequently cleared by XRN1 and the exosome.

In addition to SMG6, metazoan NMD employs SMG5 and SMG7, factors not found in *S. cerevisiae*. All three proteins act downstream of PTC recognition i.e. after deposition of the central NMD effector helicase UPF1 on the target mRNA has been triggered. They directly associate with different sections

63 of UPF1 [13], with SMG6 engaging the UPF1 N-terminus, the helicase domain [14] and a helicase
64 regulating domain [15], while the SMG5-SMG7 module recognises C-terminal (phospho-)residues
65 [16]. Historically, SMG5-SMG7 was viewed primarily as a heterodimeric adaptor that recruits general
66 mRNA turnover enzymes – including the CCR4–NOT deadenylase complex and decapping factors
67 [17-19] – thereby providing an exonucleolytic route analogous to the yeast mechanism. Although
68 early work suggested that SMG6-mediated endo-cleavage and SMG5-SMG7-mediated
69 exonucleolytic decay act in parallel and redundantly on overlapping sets of transcripts [20], more
70 recent evidence supports a linear pathway, in which SMG5-SMG7 function upstream of SMG6
71 activation [21-23]. In particular, SMG5 has been proposed to act as a licencing factor for SMG6, such
72 that SMG6 is recruited to UPF1 but requires a SMG5-SMG7-dependent authorisation step to execute
73 endonucleolytic cleavage [21]. The nature of this authorisation signal remains unknown and is
74 particularly intriguing given that, unlike SMG6, neither SMG5 nor SMG7 carry known catalytic activity
75 and are presumed to act as scaffold proteins.
76 PIN domain proteins constitute a widespread family of single-stranded RNA nucleases in prokaryotes
77 and eukaryotes. The canonical PIN core (~120-130 amino acids) adopts a conserved fold – a parallel
78 β-sheet flanked by α-helices – that forms an active site in which typically four acidic residues
79 coordinate one or more divalent metal ions (often Mg^{2+} or Mn^{2+}) to activate water for nucleophilic
80 attack and RNA cleavage [24, 25]. Early structural studies of the human (*Hs*) SMG6 PIN domain [10]
81 identified three key aspartate residues (D1251, D1353, D1392) – a reduced acidic cluster that,
82 although less common within the structurally flexible PIN family, can suffice to support metal-
83 dependent endonucleolytic activity (e.g. [26]). Indeed, *in vitro* assays demonstrated activity of a
84 recombinant wild-type SMG6 PIN domain but not a D1353A mutant [10], and in a mouse model,
85 mutation of two of the three Asp residues yielded effective NMD loss-of-function in vivo [27],
86 validating the critical role of the SMG6 aspartate triade. Intriguingly, SMG5 also carries a C-terminal
87 PIN domain with high similarity to that of SMG6, yet retains only a single conserved Asp (D860 in
88 *Hs*SMG5); consistent with an impaired catalytic site, the recombinant SMG5 PIN domain lacks
89 detectable cleavage activity [10].

90 Here, we investigate the predicted interactions among human SMG5, SMG6 and SMG7. AlphaFold3
91 [28] structure predictions recover the known SMG5-SMG7 interaction via their N-terminal domains
92 and, in addition, predict with high confidence a physical interface between the SMG5 and SMG6 PIN
93 domains that would create a composite active site. In this arrangement, a conserved aspartate from
94 SMG5 (D893) complements the SMG6 aspartate triade to yield the acidic quartet typical of canonical
95 PIN nucleases. We validate these predictions using *in vitro* nuclease assays, showing that the SMG6
96 PIN domain alone has weak nuclease activity that is ~10-fold enhanced in the presence of the SMG5
97 PIN domain. Mutational analyses further identify conserved residues required for activity of the
98 composite PIN configuration. Together, our data provide mechanistic insight into the function of the
99 previously presumed inactive SMG5 PIN domain and suggest a molecular basis for the hypothesised
100 SMG5-dependent authorisation step – namely, complementation of the SMG6 active site.

101 Results

102 Structural models predict a conserved SMG5-SMG6 PIN domain interaction

103 To explore how the metazoan-specific NMD factors SMG5, SMG6, and SMG7 assemble, we
104 performed AlphaFold3 predictions on the full-length human proteins (Figure 1 and SI Figures S1 and
105 S2). The resulting high-confidence model faithfully recapitulates the known SMG5-SMG7 complex
106 formed via their N-terminal 14-3-3-like/α-helical domains [18], as well as the established
107 intramolecular contact between the 14-3-3-like and α-helical domain of SMG6 [13] (SI Figures S1A-
108 B and S2A). Unexpectedly, however, the model simultaneously predicts a previously unrecognized
109 complex between the C-terminal PIN domains of SMG5 and SMG6 (Figure 1B). The central interface
110 is formed by interdigitating helices from both domains (SMG5 α4/5 and SMG6 α8; Figure 1D), with
111 additional predominantly hydrophobic contacts contributed by N-terminal α-helical extensions
112 (SMG5 α1 and SMG6 α1; Figure 1E, F). Moreover, a loop in SMG6 that links its 14-3-3-like and α-
113 helical domains is predicted to fold back onto the central SMG6 PIN β-sheet, contributing an extra
114 β-strand (SMG6 β1) that forms several backbone hydrogen bonds with the SMG5 PIN domain
115 (Figure 1F). While the minimal PIN-PIN interface alone covers ~70 $Å^2$, these auxialiary contacts
116 expand the putative interaction surface to ~190 $Å^2$. Importantly, this domain arrangement leaves the

117 SMG6 PIN active site fully accessible for RNA binding and even suggests that SMG5 may contribute
118 catalytically relevant residues to the ribonuclease centre (Figure 1C). To assess evolutionary
119 conservation, we generated analogous predictions for *Drosophila melanogaster* (*Dm*, for SMG5 and
120 SMG6, as no SMG7 is encoded in this organism [29]) and *Caenorhabditis elegans* (*Ce*, whose
121 orthologous proteins are considerably shorter [18]). Both species yielded closely similar
122 architectures, notably preserving the SMG5-SMG6 PIN-PIN interface and the auxiliary SMG5-6 α1
123 and SMG6 β1 contacts (SI Figures S1C-F, S2B-C and S3A-B). Consistently, sequence alignments
124 and surface mapping revealed strong conservation of interface residues in both SMG5 and SMG6,
125 as well as for the predicted SMG6 β1 strand (Figures 2B, C and SI Figure S3C).

126 **Evolutionary conservation of residues forming a putative composite SMG5-SMG6 active site**

127 The prediction that the SMG5 PIN domain sits in close proximity of the SMG6 PIN active site –
128 potentially extending several side chains into its catalytic cavity – raises the possibility that SMG5
129 contributes directly to RNA cleavage. To assess the plausibility of this model, we compared the
130 predicted SMG5-SMG6 active site configuration with canonical PIN domain family members.
131 Previous bioinformatic analyses [24, 25] identified the SMG6 PIN domain as most closely related to
132 the PIN domains of bacterial VapC toxins, which are highly active ribonucleases [26]. Structural
133 superposition of the SMG5-SMG6 PIN complex with the crystal structure of *Mycobacterium*
134 *tuberculosis* VapC3 [30]) (Figure 2A) revealed that the isolated SMG6 PIN lacks one of the four
135 conserved aspartate residues that form the catalytic tetrad (*Mt*VapC3: D4, D96, D114, D116;
136 *Hs*SMG6: D1251, D1353, D1392, **N**1394). These four Asp residues normally coordinate two divalent
137 metal ions (Mg^{2+} or Mn^{2+} in many PIN domains) that activate a nucleophilic water molecule and
138 stabilize the pentavalent transition state during phosphodiester hydrolysis. Notably, the absent fourth
139 Asp is replaced by Asn in *Hs*SMG6 and *Dm*Smg6, and even by glycine in *Ce*SMG-6 (SI Figure S3A,
140 B). Strikingly, association with SMG5 is predicted to supply a fully conserved aspartate (*Hs*SMG5
141 D893, *Dm*Smg5 D1050, *Ce*SMG-5 D464) positioned almost identically to the missing *Mt*VapC3
142 D116, thereby potentially complementing the SMG6 catalytic triad. In addition, two conserved Lys
143 sidechains of SMG5 (*Hs*SMG5 K896, K897) are predicted to reach into the active site entrance in a
144 position compatible with RNA binding; their position overlaps with an analogous Arg side chain in

145 VapC3. Together the structural models, sequence, and evolutionary comparisons support the
146 intriguing possibility that SMG5 and SMG6 cooperate to form a composite PIN-domain active site
147 that is catalytically competent for RNA cleavage.

148 **Mn^{2+}-dependent *in vitro* nuclease activity of SMG6 is enhanced by the SMG5 PIN domain**

149 Based on the above structural predictions, we next sought to validate them experimentally. We first
150 assessed the *in vitro* nuclease activity of the SMG6 PIN domain in the absence and presence of the
151 SMG5 PIN domain. Previous work by Glavan *et al.* used a gel-based assay with a radioactively end-
152 labelled U_{30} RNA oligonucleotide to measure SMG6 activity [10]. As a starting point, we developed
153 an analogous fluorescence-based assay using a modified U_{25} RNA oligonucleotide protected against
154 exonucleolytic degradation by deoxyU residues at both ends and carrying a 6-carboxyfluorescein (6-
155 FAM) label at the 5′ end (Figure 3A). In the standard assay, the probe was incubated at a 1:1 molar
156 ratio with recombinant, N-terminally tagged proteins in the presence of Mn^{2+}, and substrate turnover
157 was monitored after 45 min by 10% denaturing urea polyacrylamide gel electrophoresis (PAGE).
158 To probe the predicted SMG5-SMG6 interaction, we produced three SMG6 PIN constructs of
159 increasing length (Figure 1A and SI Figure S4): (i) a minimal PIN domain (aa 1239–1419); (ii) a short
160 extended version (aa 1162–1419), termed SMG6 PIN(α ext), which includes the predicted α-helix
161 (α1); and (iii) a long extended version (aa 567–1419), termed SMG6 PIN(14-3-3 ext), also comprising
162 the 14-3-3-like and α-helical domains that, according to the structural models, contact the PIN
163 domain through a short central β-strand (β1). The SMG5 construct used throughout (aa 827–1016,
164 termed SMG5 PIN(α ext)) was slightly longer than that used by Glavan *et al.* (aa 853–1016; [10]), as
165 it included the predicted α-helical extension (α1), which in the structural models forms stabilizing
166 contacts with the SMG6 α1 helix to reinforce the PIN-PIN interface.
167 Side-by-side comparisons revealed that the SMG6 PIN(14-3-3 ext) construct combined with SMG5
168 PIN(α ext) exhibited the highest activity, achieving near-complete substrate degradation (~95%
169 turnover after 45 min; Figure 3B, lanes 11-12; Figure 3C). Notably, this SMG6 construct also
170 displayed substantial basal activity in the absence of SMG5 (~50% turnover; lanes 9-10). By
171 contrast, combining SMG5 with shorter SMG6 constructs yielded progressively weaker activity: the

172 minimal SMG6 PIN and SMG6 PIN(α ext) constructs turned over only ~20% and ~30% of substrate,
173 respectively (lanes 1-8), and both constructs were essentially inactive without SMG5 (Figure 3C).
174 All assays were conducted in the presence of Mn^{2+}, the preferred cofactor for many PIN domain
175 nucleases. Using the SMG5 PIN(α ext)-SMG6 PIN(14-3-3 ext) combination, we verified metal ion
176 specificity: substituting Mn^{2+} with Mg^{2+} or Zn^{2+} abolished cleavage, and chelation with EDTA blocked
177 Mn^{2+}-dependent degradation (Figure 3D, E).
178 In summary, SMG5 PIN markedly enhances SMG6 PIN nuclease activity *in vitro*, and structural
179 extensions on SMG6 make substantial contributions to achieving maximal activity.

180 **Extended SMG5-SMG6 contacts can be functionally mimicked by covalent tethering**

181 Our initial interpretation of the high activity observed with the structurally extended SMG6 construct
182 was that the additional sequences stabilise a PIN-PIN interaction between SMG5 and SMG6 that
183 would otherwise be weak. However, we could not exclude the possibility that these SMG6 extensions
184 contribute directly to catalysis or RNA binding rather than acting solely as structural stabilisers.
185 To discriminate between these possibilities, we used the SMG5 PIN(α ext) and the SMG6 PIN(α ext)
186 constructs, which exhibited low activity in our assays (Figure 3B, lanes 7-8; Figure 3C), and
187 irreversibly linked them into a single polypeptide using the SpyTag/SpyCatcher system [31].
188 Remarkably, the covalently tethered SMG5-SMG6 pair displayed markedly higher activity than the
189 corresponding non-tethered proteins. In fact, the SpyTag/SpyCatcher-linked SMG5 PIN(α ext)-
190 SMG6 PIN(α ext) construct approached the activity of the unlinked SMG5 PIN(α ext)-SMG6 PIN(14-
191 3-3 ext) proteins (Figure 4A, B). These findings indicate that the additional SMG6 sequences
192 primarily act to stabilise SMG5-SMG6 association and become dispensable when physical proximity
193 is enforced by other means. In our assay, this was achieved via covalent linkage; *in vivo*, an
194 analogous effect may be mediated by co-recruitment of SMG5 and SMG6 to the common binding
195 platform, phospho-UPF1.
196 As a second, orthogonal test of the predicted weak interaction, we assessed the temperature-
197 dependence of SMG5-SMG6 activity. Our rationale was that temperature exerts opposing effects on
198 two key factors: enzymatic kinetics and protein-protein interaction. Lower temperatures generally
199 slow catalytic turnover but can stabilise weak interfaces, whereas higher temperatures accelerate

intrinsic reaction rates yet destabilise fragile interactions. Thus, if SMG5 and SMG6 interact weakly, we would expect increased activity at low temperature (due to improved complex stability) and reduced activity at high temperature, despite faster kinetics. Conversely, a strongly interacting dimer would be expected to show the opposite trend – slower activity at low temperature and faster at high temperature.

We tested this by performing the *in vitro* cleavage assay at four temperatures: 0 °C (on ice), 10 °C, 37 °C (as in Figure 3B), and 42 °C (proxy for upper physiological limit in humans). The results were unambiguous: low temperatures strongly enhanced substrate turnover by SMG6 variants that were nearly inactive at 37 °C. For example, the SMG6 PIN(α ext) together with SMG5 PIN(α ext) degraded only ~30-40% of substrate at 37 °C–42 °C but achieved 80-90% turnover at 0 °C–10 °C (Figure 4C, lanes 7-8; Figure 4D). Additional observations from the temperature experiment included: (i) even the minimal SMG6 PIN acquired measurable activity with SMG5 at 0°C (30-40% turnover; lanes 3-4); and (ii) basal activity of SMG6 constructs alone also increased at low temperature – for instance, SMG6 PIN(14-3-3 ext) turned over ~60% of substrate at 37 °C but 70-90% at 0 °C–10 °C (lanes 9-10). These temperature-dependent improvements may reflect enhanced RNA binding or improved structural stability and/or Mn^{2+} coordination at low temperature.

Together, these results demonstrate that the SMG5-SMG6 PIN domains form a weak, temperature-sensitive interaction that can be functionally stabilised either by extended structural elements or by enforced physical proximity. This supports a model in which auxiliary contacts on SMG6 reinforce the composite active site formed with SMG5.

Quantitative comparison of nuclease kinetics through a real-time fluorescent cleavage assay

The gel-based endpoint assays above provided important insights into SMG6 nuclease activity and its modulation by SMG5, but they were unsuitable for kinetic analysis. To enable quantitative rate measurements, capture early reaction phases, and increase throughput, we developed a fluorescence-based real-time cleavage assay. This platform is particularly advantageous for analysing subtle effects of protein mutations on nuclease activity. We used a modified U_{25} RNA oligonucleotide substrate carrying a 6-FAM fluorophore at the 5′ end and a Black Hole Quencher 1

227 (BHQ1) at the 3′ end. In the intact substrate, BHQ1 quenches the 6-FAM signal, while cleavage
228 separates the two moieties and results in increased fluorescence (Figure 5A).
229 We benchmarked our assay using conditions similar to the gel-based assay. Reactions were initiated
230 by protein addition, and fluorescence was recorded every minute for 60 min using a plate reader.
231 The assay reproduced all preceding findings while enabling precise kinetic comparisons. SMG5
232 PIN(α ext) with SMG6 PIN(14-3-3 ext) and the SpyTag/SpyCatcher-tethered SMG5-SMG6 pair were
233 highly active, reaching 50% substrate turnover in <5 min (Figure 5B). SMG6 PIN(14-3-3 ext) alone
234 displayed clear activity but required >20 min to reach 50% turnover, whereas SMG5 PIN(α ext) with
235 SMG6 PIN(α ext) showed only weak activity and all other constructs were inactive.
236 We fitted the fluorescence curves with a single-exponential model to derive apparent rate constants
237 (k_{obs}). The most active constructs yielded k_{obs} values of ~0.2 min^{-1}, whereas SMG6 PIN(14-3-3 ext)
238 alone was almost 7-fold slower ($k_{obs} \approx 0.03$ min^{-1}) (Figure 5C).
239 In summary, this real-time assay provides fine-resolution kinetic measurements and a robust
240 platform for dissecting SMG5/SMG6 function and mutant phenotypes.

241 **Mutational analysis validates SMG5-contributed active site residues and the SMG5-SMG6**
242 **interaction surface**

243 To validate the structural model, we generated SMG5 and SMG6 mutants targeting two features: the
244 composite active site (Figures 1C and 6A) and the predicted PIN-PIN interface (Figures 1D and 6B).
245 First, we probed the composite active site. Recombinant SMG6 PIN(14-3-3 ext) carrying a D1353A
246 mutation was nucleolytically inactive in all conditions, confirming the essential role of this catalytic
247 residue (Figure 6A, C). On the SMG5 side, converting D893 to alanine abolished the ability of SMG5
248 PIN(α ext) to enhance SMG6-mediated cleavage, consistent with its proposed role in complementing
249 the active site. Furthermore, mutating the conserved K896 and K897 – located near the composite
250 active site and potentially involved in RNA binding – also eliminated SMG5-mediated stimulation.
251 Analogous results were found for these mutants in the SpyTag/SpyCatcher setup (SI Figure S5A,
252 B).
253 Next, we interrogated the predicted interaction surface. Structural models suggested an electrostatic
254 contact between SMG5 E910 and SMG6 R1396 (Figure 1D). Disrupting this interaction by charge

255 reversal (SMG5 E910R or SMG6 R1396E, together with a WT partner protein) greatly reduced
256 activity (k_{obs} ≈ 0.03 min^{-1} and 0.01 min^{-1}, respectively), compared with that of the two WT proteins
257 (k_{obs} ≈ 0.25 min^{-1}; Figure 6B, D). Strikingly, combining both mutants (SMG5 E901R + SMG6 R1396E)
258 restored activity almost fully (k_{obs} ≈ 0.17 min^{-1}), directly validating the predicted electrostatic
259 interaction. A second interface mutant, SMG6 V1397E, also prevented SMG5-mediated stimulation
260 (SI Figure S5C-F). Interestingly, both SMG6 interface mutants reduced basal activity even in the
261 absence of SMG5, conceivably because introducing a negative charge (glutamate) near the active
262 site could perturb RNA binding.
263 In summary, these mutational analyses confirm the structural model of active site complementation
264 between SMG5 and SMG6 and identify conserved residues critical for catalysis and PIN–PIN
265 interaction.

266 Discussion

267 The precise roles of SMG5, SMG6, and SMG7 in the effector phase of metazoan NMD have
268 remained unclear for decades. While SMG6 was established as the pathway's dedicated
269 endonuclease, SMG5 and SMG7 were largely considered scaffolds that recruit general decay factors
270 such as deadenylases and decapping enzymes. Our findings revise this view by demonstrating that
271 SMG5 directly contributes to catalysis: its PIN domain complements residues missing from the
272 SMG6 active site, generating a composite nuclease architecture. This mechanism explains why the
273 isolated SMG6 PIN domain is unable to trigger mRNA decay *in vivo* even upon tethering [32], why
274 SMG5 acts as a licensing factor for SMG6 [22, 23], and it provides a molecular basis for the proposed
275 authorisation step in NMD [21]. Together with prior literature, our data supports a model in which the
276 SMG5-SMG7 heterodimer is recruited efficiently to the phosphorylated C-terminus of UPF1 via its
277 two adjacent 14-3-3-like domains [13, 16, 18, 33, 34], while SMG6 recognizes both the RNA-bound
278 conformation of UPF1 and its phosphorylated N-terminus [13-15]. Only the avidity afforded by this
279 combination of several low affinity interactions brings the two PIN domains of SMG6 and SMG5 into
280 proximity to elicit stable active site formation and productive RNA cleavage (Figure 6E). The
281 intramolecular connection between the SMG6 14-3-3-like domain and its PIN domain may help

ensure that cleavage occurs *in cis*, in close proximity to the UPF1 RNA binding site and the PTC [12, 35].

Composite active sites are not unprecedented in the PIN domain superfamily. Structural studies of bacterial VapC toxins and other PIN-containing effectors have shown that dimerization configures catalytic grooves, often bringing together acidic residues from two domains [26, 36]. Similar principles underlie many PIN-domain and related nucleases, where catalysis is conditional upon oligomerization or conformational change. For instance, CRISPR-associated PIN enzymes can be activated by cyclic tetraadenylate (cA_4)-dependent oligomerization that reconfigures active-site residues across different subunits [37]. Our work extends this paradigm to eukaryotic RNA surveillance, revealing that SMG5 and SMG6 cooperate to assemble a canonical PIN active site that neither domain can fully provide alone.

This conditional assembly offers an elegant regulatory strategy. Nuclease activation is contingent upon protein-protein interactions and co-recruitment to a common platform – phosphorylated [13, 16] and RNA-bound [15] UPF1 – ensuring tight spatial and temporal control during NMD. The requirement for SMG5-mediated complementation effectively establishes a checkpoint that licences SMG6 activity only within correctly assembled surveillance complexes. Such conditional activation also prevents ectopic SMG6 activity in the cytoplasm, safeguarding transcripts from unintended cleavage.

Evolutionary comparisons reinforce this model. *Drosophila melanogaster* lacks SMG7 but retains SMG5 and SMG6 [29], suggesting that the SMG5-SMG6 partnership represents the catalytic core of metazoan NMD. SMG7 may represent an additional, yet dispensable adaptor to enhance exonucleolytic decay or pathway regulation, whereas SMG5's contribution to SMG6 activation appears indispensable. This observation underscores that SMG5 is not merely a scaffold but a critical licensing factor for SMG6 endonucleolytic activity.

Beyond clarifying SMG5's role, these findings highlight composite PIN architectures as a recurrent evolutionary solution for licensing nuclease activity. Conditional assembly allows organisms to couple catalytic potency to molecular context, a principle that may apply broadly to RNA decay pathways and other nucleases. Future work should examine whether SMG7 contributes additional

310 layers of regulation, how UPF1 phosphorylation dynamics influence composite active site formation,
311 and whether similar composite architectures exist in other metazoan RNA surveillance systems.
312 Understanding these mechanisms will not only refine models of NMD regulation but may also inform
313 therapeutic strategies targeting aberrant RNA decay in genetic disease and cancer.

314 Methods

315 Cloning

316 Human *SMG5* and *SMG6* sequences were amplified by PCR from plasmids pcDNA3.1-MS2-HA-
317 HsSmg5_T (Addgene #147552) [19] and pCIneo-λN-HA-HsSmg6_I (Addgene #146551) [38], or
318 from HEK293 cell cDNA, and then cloned by Golden-gate cloning into low-copy plasmid pLIBT7 in
319 fusion with N-terminal His-tag (for SMG5), N-terminal HisGST-tag (for SMG6), N-terminal SpyTag
320 [31] and C-terminal His-tag (for SMG5) or N-terminal SpyCatcher [31] and C-terminal His-tag (for
321 SMG6). For bacterial co-expression, SMG5 plasmids carried ampicillin resistance and SMG6
322 plasmids kanamycin resistance. To generate specific amino acid mutations, we used the classical
323 QuikChange site-directed mutagenesis protocol based on polymerase chain reaction (PCR)
324 amplification using *Pfu*Turbo DNA polymerase (Agilent) and two complementary oligonucleotide
325 primers (Microsynth) containing the desired mutation. Following temperature cycling, reactions were
326 treated with *Dpn*I (New England Biolabs) for digestion of parental DNA template. After transformation
327 (XL2-Blue), positive clones were identified and validated by Sanger sequencing. Oligos used for
328 mutagenesis are as follows, with lowercase letters indicating mutated nucleotides:

Protein	Mutation	Oligo sequences (5' to 3'), upper and lower oligos
SMG5	D893A	CCCAAGGACAGTGATCGATGGgCTagctTTGCTGAAGAAGGAACACCCAG CTGGGTGTTCCTTCTTCAGCAAagctAGcCCATCGATCACTGTCCTTGGG
SMG5	E910R	GGGATTCGGTACCTGcgcGCAGAGTTTAAAAAAGGAAAC GTTTCCTTTTTTAAACTCTGCgcgCAGGTACCGAATCCC
SMG5	K896A,K897A	GATGGCCTGGATTTGCTGgctgcaGAACACCCAGGGGCCCGG CCGGGCCCCTGGGTGTTCtgcagcCAGCAAATCCAGGCCATC
SMG6	D1353A	GGCCAGCTGGGTAACAACGcaGATCTCATCCTGTCCTGCT GCAGGACAGGATGAGATCtgCGTTGTTACCCAGCTGGC
SMG6	R1396E	GACGGATGACCGGAACCTcgagGTGAAGGCGCTCACAAG CTTGTGAGCGCCTTCACctcgAGGTTCCGGTCATCCGTC
SMG6	V1397E	CGGAACCTGCGTGagAAGGCGCTCACAAGGAA TTCCTTGTGAGCGCCTTctCACGCAGGTTCCG

329 The overall list of DNA constructs used in this study is as follows:

330 pLIBT7_A_HisHsSMG5(827-C)

331 pLIBT7_A_HisHsSMG5(827-C)_D893A

332 pLIBT7_A_HisHsSMG5(827-C)_E910R

333 pLIBT7_A_HisHsSMG5(827-C)_K896A, K897A

334 pLIBT7_A_SpyTag-SMG5(827-C)-His

335 pLIBT7_A_SpyTag-SMG5(827-C)-His_D893A

336 pLIBT7_A_SpyTag-SMG5(827-C)-His_K896A, K897A

337 pLIBT7_K_HisGST-TEV-SMG6(1162-C)

338 pLIBT7_K_HisGST-TEV-SMG6(567-C)

339 pLIBT7_K_HisGST-TEV-SMG6(567-C)_D1353A

340 pLIBT7_K_HisGST-TEV-SMG6(567-C)_R1396E

341 pLIBT7_K_HisGST-TEV-SMG6(567-C)_V1397E

342 pLIBT7_K_SpyCatcher-SMG6(1162-C)-His

343 pLIBT7_K_SpyCatcher-SMG6(1162-C)-His_D1353A

344 pLIBT7_K_SpyCatcher-SMG6(1162-C)-His_V1397E

345 **Expression, and purification of SMG5 and SMG6 proteins**

346 Pairs of SMG5- and SMG6-expression plasmids were co-transformed into electrocompetent *E. coli*
347 Rosetta(DE3) cells and positive clones were selected on LB plates supplemented with 100 µg/mL
348 ampicillin, 50 µg/mL kanamycin, and 30 µg/mL chloramphenicol. These cells were used to inoculate
349 1 L cultures in TB medium, and after growth at 37 °C to an OD600 of 0.5-1 the temperature was
350 reduced to 22 °C. Expression was then induced by addition of IPTG to a final concentration of
351 0.4 mM, and the cultures were left shaking at 22 °C overnight (16 h). Bacteria were collected by
352 centrifugation and the pellet was resuspended in 70 mL of Lysis buffer (50 mM Tris-HCl pH 7.5,
353 300 mM NaCl, 5% glycerol, 25 mM imidazole) supplemented with 5 mM β-mercaptoethanol and
354 protease inhibitors (Roche). Cells were lysed by sonication on ice (Bandelin sonicator equipped with
355 VS70T-tip) for 12 min total sonication time (40% output, pulsing 1 s ON / 1 s OFF) and the lysate
356 was clarified by centrifugation at 40000× *g* at 4 °C for 30 min. This lysate was then loaded on a 5 mL
357 HisTrap-HP column (Cytiva) equilibrated in Lysis buffer, followed by a 6 column volume (cV) wash

358 with Lysis buffer. Bound material was then eluted with a 10 cV gradient from Lysis buffer to the same
359 buffer supplemented with 500 mM imidazole. His-GST-TEV-SMG6 and His-SMG5 proteins eluted in
360 separate but overlapping peaks, indicating that their interaction was too weak to fully withstand this
361 purification at 300 mM NaCl concentration. Fractions containing the desired proteins were
362 nevertheless pooled, concentrated to a volume of around 500 µL, and injected onto a Superdex200
363 Increase size-exclusion column equilibrated in SEC buffer (20 mM Tris-HCl pH 7.5, 250 mM NaCl).
364 His-GST-TEV-SMG6 and His-SMG5 proteins eluted in distinct peaks, which were individually pooled
365 and concentrated. The obtained protein solutions were aliquoted, snap-frozen in liquid nitrogen, and
366 stored at -70 °C.

367 **Expression and purification of SpyTag-SMG5/SpyCatcher-SMG6 pairs**

368 Combinations of the desired plasmid were co-transformed into *E. coli* Rosetta(DE3) and cultures
369 were grown and lysed as described above. After loading on a His-Trap column the dimer eluted
370 slightly separated from excess SpyTag-SMG5 protein, and fractions containing the desired dimer
371 were concentrated to 500 µL followed by Superdex200 Increase size-exclusion chromatography as
372 described above. The dimer eluted well-separated from the remaining excess SpyTag-SMG5 protein,
373 and was concentrated, aliquoted, snap-frozen and stored at -70 °C.

374 ***In vitro* gel-based nuclease assay**

375 In a reaction volume of 5 µL, 3 µM of 5'-6FAM-dU-U_{25}-dU-oligo (IDT) was incubated with 3 µM of
376 recombinant proteins in reaction buffer containing 100 mM NaCl, 10% glycerol, 5 mM $MnCl_2$, 25 mM
377 Tris-HCl pH 7.5, 1 mM DTT. In some assays (e.g., to show the specificity of Mn^{2+}-based RNA
378 degradation) 1 mM EGTA and/or 30 mM EDTA were added. The reaction mix was then incubated at
379 temperatures indicated in figure legends (42 °C, 37 °C, 10 °C, or 0 °C), for a reaction time of 45 min
380 (or for 0 min for control sample). After incubation, each reaction was first mixed with 5 µL of 2x RNA
381 loading dye (95% formamide, 18 mM EDTA, 0.025% SDS, and Bromophenol Blue), then heated at
382 95 °C for 5 min, chilled on ice, then loaded on a 10% polyacrylamide gel containing 7 M Urea
383 (Invitrogen, EC68755BOX). Gel electrophoresis was performed at 120 V for 50 min.

384 ***In vitro* kinetic nuclease assay**

385 Using substrate concentration of 3 µM for the fluorescence-quenched oligo 5'-6FAM-dU-U_{25}-dU-3'-
386 BHQ1 (IDT) and 3 µM of recombinant proteins (or RNase-free water as negative control), reactions
387 were carried out in 10 µL and reaction buffer 100 mM NaCl, 10% glycerol, 5 mM $MnCl_2$, 1 mM EGTA,
388 25 mM Tris-HCl pH 7.5, 1 mM DTT. To catch early reaction timepoints reliably, reactions were
389 typically started by adding the proteins as the last component. The reaction was then incubated at
390 25 °C for 60 min in a flat-bottom black 384-well plate (Corning). Fluorescence signal was measured
391 every minute in a plate reader (Tecan Safire 2). To calculate observed reaction rate constants (k_{obs}),
392 within one experiment (i.e., on the same plate) raw data were first normalised to 0-100%, followed
393 by non-linear curve fit (single exponential growth to plateau, using GraphPad Prism 10 software)
394 with formula $Y=100 * (1 - \exp(-k_{obs} * X))$. As we noted that bleaching of signal occurred over time
395 (i.e., 100% signal decays), we also tried curve fit formulas with a bleaching term, but as the obtained
396 k_{obs} values were near-identical to the simple fits, we report the outcomes from the simple model in
397 this study.

398 **Structure predictions**

399 AlphaFold3 [28] was used for structure predictions (5 models each) of complexes formed by full
400 length human (*Hs*) SMG5-6-7, *Drosophila melanogaster* (*Dm*) Smg5-6 (no Smg7 ortholog present
401 in flies), or *Caenorhabditis elegans* (*Ce*) SMG-5-6-7 each including U_6 RNA and 2 Mg^{2+}. The highest
402 ranked model of each prediction was used for visualizations with ChimeraX1.10 [39]. Predicted
403 Aligned Error (PAE) plots were generated with PAE viewer [40], while surface conservation scores
404 were calculated using ConSurf [41] with structure models as input and default settings.

405 **Sequence alignments**

406 Sequences of human SMG5, SMG6 and orthologous proteins were identified via TreeFam [42] or by
407 BLAST search [43] and aligned using the MUSCLE webserver [44] from within JALVIEW [45].
408 Positional conservation and similarity scores were calculated using the ESPRIPT webserver [46]
409 with default settings.

410 CRediT authorship contribution statement

Enes S. Arpa: Writing – review & editing, Writing – original draft, Visualization, Validation, Conceptualization, Formal analysis, Investigation, Methodology. **Michael Taschner:** Writing – review & editing, Writing – original draft, Conceptualization, Investigation, Methodology. **Mara De Matos:** Investigation, Methodology. **Stefanie Jonas:** Writing – review & editing, Writing – original draft, Visualization, Funding acquisition, Conceptualization, Methodology, Supervision. **David Gatfield:** Writing – review & editing, Writing – original draft, Visualization, Funding acquisition, Conceptualization, Formal analysis, Supervision, Project administration.

Declaration of competing interest

The authors declare that they have no known competing financial interests or personal relationships that could have appeared to influence the work reported in this paper.

Acknowledgements

This work was supported by the University of Lausanne and ETH Zurich, Swiss National Science Foundation (SNSF) NCCR RNA & Disease Phase III funding (grant number 205601 to D.G. and S.J.), SNSF Project funding (grant number 212423 to D.G., and 207458 to S.J.), an ERC Consolidator grant funded via SERI (MB22.00064 to S.J.), an EMBO Young Investigators Award (4918 to S.J.).

427 ## References

428 [1] Peltz SW, Brown AH, Jacobson A. mRNA destabilization triggered by premature translational
429 termination depends on at least three cis-acting sequence elements and one trans-acting factor.
430 Genes & development. 1993;7:1737-54.

431 [2] Leeds P, Peltz SW, Jacobson A, Culbertson MR. The product of the yeast UPF1 gene is required
432 for rapid turnover of mRNAs containing a premature translational termination codon. Genes &
433 development. 1991;5:2303-14.

434 [3] Hodgkin J, Papp A, Pulak R, Ambros V, Anderson P. A new kind of informational suppression in
435 the nematode Caenorhabditis elegans. Genetics. 1989;123:301-13.

436 [4] He F, Jacobson A. Upf1p, Nmd2p, and Upf3p regulate the decapping and exonucleolytic
437 degradation of both nonsense-containing mRNAs and wild-type mRNAs. Molecular and cellular
438 biology. 2001;21:1515-30.

439 [5] Lejeune F, Li X, Maquat LE. Nonsense-mediated mRNA decay in mammalian cells involves
440 decapping, deadenylating, and exonucleolytic activities. Molecular cell. 2003;12:675-87.

441 [6] Karousis ED, Muhlemann O. The broader sense of nonsense. Trends in biochemical sciences.
442 2022;47:921-35.

443 [7] Muhlrad D, Parker R. Premature translational termination triggers mRNA decapping. Nature.
444 1994;370:578-81.

445 [8] Mitchell P, Tollervey D. An NMD pathway in yeast involving accelerated deadenylation and
446 exosome-mediated 3'-->5' degradation. Molecular cell. 2003;11:1405-13.

447 [9] Gatfield D, Izaurralde E. Nonsense-mediated messenger RNA decay is initiated by
448 endonucleolytic cleavage in Drosophila. Nature. 2004;429:575-8.

449 [10] Glavan F, Behm-Ansmant I, Izaurralde E, Conti E. Structures of the PIN domains of SMG6 and
450 SMG5 reveal a nuclease within the mRNA surveillance complex. The EMBO journal.
451 2006;25:5117-25.

452 [11] Huntzinger E, Kashima I, Fauser M, Sauliere J, Izaurralde E. SMG6 is the catalytic endonuclease
453 that cleaves mRNAs containing nonsense codons in metazoan. Rna. 2008;14:2609-17.

454 [12] Eberle AB, Lykke-Andersen S, Muhlemann O, Jensen TH. SMG6 promotes endonucleolytic
455 cleavage of nonsense mRNA in human cells. Nature structural & molecular biology. 2009;16:49-
456 55.
457 [13] Chakrabarti S, Bonneau F, Schussler S, Eppinger E, Conti E. Phospho-dependent and phospho-
458 independent interactions of the helicase UPF1 with the NMD factors SMG5-SMG7 and SMG6.
459 Nucleic acids research. 2014;42:9447-60.
460 [14] Barbarin-Bocahu I, Ulryck N, Rigobert A, Ruiz Gutierrez N, Decourty L, Raji M, et al. Structure
461 of the Nmd4-Upf1 complex supports conservation of the nonsense-mediated mRNA decay
462 pathway between yeast and humans. PLoS biology. 2024;22:e3002821.
463 [15] Langer LM, Kurscheidt K, Basquin J, Bonneau F, Iermak I, Basquin C, et al. UPF1 helicase
464 orchestrates mutually exclusive interactions with the SMG6 endonuclease and UPF2. Nucleic
465 acids research. 2024;52:6036-48.
466 [16] Okada-Katsuhata Y, Yamashita A, Kutsuzawa K, Izumi N, Hirahara F, Ohno S. N- and C-terminal
467 Upf1 phosphorylations create binding platforms for SMG-6 and SMG-5:SMG-7 during NMD.
468 Nucleic acids research. 2012;40:1251-66.
469 [17] Unterholzner L, Izaurralde E. SMG7 acts as a molecular link between mRNA surveillance and
470 mRNA decay. Molecular cell. 2004;16:587-96.
471 [18] Jonas S, Weichenrieder O, Izaurralde E. An unusual arrangement of two 14-3-3-like domains in
472 the SMG5-SMG7 heterodimer is required for efficient nonsense-mediated mRNA decay. Genes
473 & development. 2013;27:211-25.
474 [19] Loh B, Jonas S, Izaurralde E. The SMG5-SMG7 heterodimer directly recruits the CCR4-NOT
475 deadenylase complex to mRNAs containing nonsense codons via interaction with POP2. Genes
476 & development. 2013;27:2125-38.
477 [20] Colombo M, Karousis ED, Bourquin J, Bruggmann R, Muhlemann O. Transcriptome-wide
478 identification of NMD-targeted human mRNAs reveals extensive redundancy between SMG6-
479 and SMG7-mediated degradation pathways. Rna. 2017;23:189-201.

480 [21] Boehm V, Kueckelmann S, Gerbracht JV, Kallabis S, Britto-Borges T, Altmuller J, et al. SMG5-
481 SMG7 authorize nonsense-mediated mRNA decay by enabling SMG6 endonucleolytic activity.
482 Nature communications. 2021;12:3965.
483 [22] Huth M, Santini L, Galimberti E, Ramesmayer J, Titz-Teixeira F, Sehlke R, et al. NMD is required
484 for timely cell fate transitions by fine-tuning gene expression and regulating translation. Genes
485 & development. 2022;36:348-67.
486 [23] Viscardi MJ, Sehgal E, Arribere JA. Endonucleolytic cleavage is the primary mechanism of
487 decay elicited by C. elegans nonsense-mediated mRNA decay. Genome research.
488 2025;35:1337-48.
489 [24] Senissar M, Manav MC, Brodersen DE. Structural conservation of the PIN domain active site
490 across all domains of life. Protein Sci. 2017;26:1474-92.
491 [25] Matelska D, Steczkiewicz K, Ginalski K. Comprehensive classification of the PIN domain-like
492 superfamily. Nucleic acids research. 2017;45:6995-7020.
493 [26] Arcus VL, McKenzie JL, Robson J, Cook GM. The PIN-domain ribonucleases and the
494 prokaryotic VapBC toxin-antitoxin array. Protein Eng Des Sel. 2011;24:33-40.
495 [27] Katsioudi G, Dreos R, Arpa ES, Gaspari S, Liechti A, Sato M, et al. A conditional Smg6 mutant
496 mouse model reveals circadian clock regulation through the nonsense-mediated mRNA decay
497 pathway. Sci Adv. 2023;9:eade2828.
498 [28] Abramson J, Adler J, Dunger J, Evans R, Green T, Pritzel A, et al. Accurate structure prediction
499 of biomolecular interactions with AlphaFold 3. Nature. 2024;630:493-500.
500 [29] Gatfield D, Unterholzner L, Ciccarelli FD, Bork P, Izaurralde E. Nonsense-mediated mRNA
501 decay in Drosophila: at the intersection of the yeast and mammalian pathways. The EMBO
502 journal. 2003;22:3960-70.
503 [30] Das U, Pogenberg V, Subhramanyam UK, Wilmanns M, Gourinath S, Srinivasan A. Crystal
504 structure of the VapBC-15 complex from Mycobacterium tuberculosis reveals a two-metal ion
505 dependent PIN-domain ribonuclease and a variable mode of toxin-antitoxin assembly. J Struct
506 Biol. 2014;188:249-58.

507 [31] Zakeri B, Fierer JO, Celik E, Chittock EC, Schwarz-Linek U, Moy VT, et al. Peptide tag forming
508 a rapid covalent bond to a protein, through engineering a bacterial adhesin. Proceedings of the
509 National Academy of Sciences of the United States of America. 2012;109:E690-7.
510 [32] Nicholson P, Josi C, Kurosawa H, Yamashita A, Muhlemann O. A novel phosphorylation-
511 independent interaction between SMG6 and UPF1 is essential for human NMD. Nucleic acids
512 research. 2014;42:9217-35.
513 [33] Fukuhara N, Ebert J, Unterholzner L, Lindner D, Izaurralde E, Conti E. SMG7 is a 14-3-3-like
514 adaptor in the nonsense-mediated mRNA decay pathway. Molecular cell. 2005;17:537-47.
515 [34] Durand S, Franks TM, Lykke-Andersen J. Hyperphosphorylation amplifies UPF1 activity to
516 resolve stalls in nonsense-mediated mRNA decay. Nature communications. 2016;7:12434.
517 [35] Boehm V, Haberman N, Ottens F, Ule J, Gehring NH. 3' UTR length and messenger
518 ribonucleoprotein composition determine endocleavage efficiencies at termination codons. Cell
519 reports. 2014;9:555-68.
520 [36] Cook GM, Robson JR, Frampton RA, McKenzie J, Przybilski R, Fineran PC, et al. Ribonucleases
521 in bacterial toxin-antitoxin systems. Biochimica et biophysica acta. 2013;1829:523-31.
522 [37] Wang F, Zhao P, Bi X, Zheng R, Tian X, Xu J, et al. Cyclic tetraadenylate binding induces
523 dimerization of protein dimers to activate a CRISPR-associated PIN nuclease. Nucleic acids
524 research. 2025;53.
525 [38] Kashima I, Jonas S, Jayachandran U, Buchwald G, Conti E, Lupas AN, et al. SMG6 interacts
526 with the exon junction complex via two conserved EJC-binding motifs (EBMs) required for
527 nonsense-mediated mRNA decay. Genes & development. 2010;24:2440-50.
528 [39] Meng EC, Goddard TD, Pettersen EF, Couch GS, Pearson ZJ, Morris JH, et al. UCSF ChimeraX:
529 Tools for structure building and analysis. Protein Sci. 2023;32:e4792.
530 [40] Elfmann C, Stulke J. PAE viewer: a webserver for the interactive visualization of the predicted
531 aligned error for multimer structure predictions and crosslinks. Nucleic acids research.
532 2023;51:W404-W10.

533 [41] Yariv B, Yariv E, Kessel A, Masrati G, Chorin AB, Martz E, et al. Using evolutionary data to make
534 sense of macromolecules with a "face-lifted" ConSurf. Protein Sci. 2023;32:e4582.
535 [42] Ruan J, Li H, Chen Z, Coghlan A, Coin LJ, Guo Y, et al. TreeFam: 2008 Update. Nucleic acids
536 research. 2008;36:D735-40.
537 [43] Altschul SF, Madden TL, Schaffer AA, Zhang J, Zhang Z, Miller W, et al. Gapped BLAST and
538 PSI-BLAST: a new generation of protein database search programs. Nucleic acids research.
539 1997;25:3389-402.
540 [44] Edgar RC. MUSCLE: multiple sequence alignment with high accuracy and high throughput.
541 Nucleic acids research. 2004;32:1792-7.
542 [45] Waterhouse AM, Procter JB, Martin DM, Clamp M, Barton GJ. Jalview Version 2--a multiple
543 sequence alignment editor and analysis workbench. Bioinformatics. 2009;25:1189-91.
544 [46] Robert X, Gouet P. Deciphering key features in protein structures with the new ENDscript server.
545 Nucleic acids research. 2014;42:W320-4.

546 ## Figure Legends

547 **Figure 1. Structure models of SMG5 and SMG6 predict formation of a composite PIN domain.**
548 (**A**) Schematic domain architecture of *Hs*SMG5 and SMG6. SMG6 binding motifs for exon junction
549 complex (EBMs 39-59 and 133-153) and UPF1 (U1BM 406-419 and ARM 445-465) are indicated by
550 spheres. Constructs used in the study, i.e. SMG5 PIN(α extension) (827-C), SMG6 PIN(minimal)
551 (1239-C), SMG6 PIN(α extension) (1162-C) and SMG6 PIN(14-3-3 extension) (567-C), are indicated
552 at the bottom of each cartoon. The α-helices located N-terminally to the PIN domains that are
553 predicted to interact are highlighted in colour and labelled α1. The β-strand, which is inserted in a
554 loop between SMG6 14-3-3-like (14-3-3) and α-helical (αH) domain and which is predicted to
555 intramolecularly complement the PIN-domain β-sheet is indicated as β1.
556 (**B**) Model of the complex between *Hs*SMG5 PIN domain (purple, pink) and the folded domains of
557 *Hs*SMG6 (shades of green) based on an AlphaFold3 model of the *Hs*SMG5-6-7 complex with U_6-
558 RNA and 2 Mg^{2+}. Domains are coloured as in (A). RNA (grey) and metal ions (yellow spheres) in the
559 active site are shown. Elements that contribute to the interaction i.e. α1-helices and β1-strand are
560 highlighted and labelled.
561 (**C**) Zoom into the proposed composite active site. Active site residues of SMG6 (green) and SMG5
562 (purple) are shown as sticks and labelled. Residues mutated in this study are underlined. Predicted
563 positions of two bivalent cations (M^{2+}) that are coordinated by the acidic residues, as well as three
564 nucleotides of RNA substrate (dark grey) are also shown. Dotted lines indicate putative hydrogen
565 bonds and salt bridges.
566 (**D**) Zoom into the *Hs*SMG5PIN-SMG6PIN interface viewed from the bottom of the active site shown
567 in (C). Residues of SMG5 (purple) and SMG6 (green) that are predicted to contribute to binding are
568 shown as sticks and labelled. Residues mutated in the study are underlined. Dotted lines indicate
569 putative hydrogen bonds or salt bridges.
570 (**E**) Predicted interface between α-helical extensions (α1) of *Hs*SMG5 (pink) and SMG6 (light green)
571 PIN domains. Interface residues are shown as sticks and labelled.
572 (**F**) Predicted interface between SMG6 α1 (light green) and β1 with SMG5PIN (purple). Dotted lines
573 indicate putative hydrogen bonds or salt bridges.

574 **Figure 2. The composite SMG5-6 PIN active site and domain interface are evolutionarily**
575 **conserved.**
576 (**A**) Superposition of the crystal structure of prototypical PIN domain family member *Mt*VapC3 (light
577 grey, PDB ID 4CHG)[30] shows that it displays a similar arrangement of active site residues as the
578 composite SMG5-6 PIN domain. Active site residues are shown as sticks and labelled. The two metal
579 ions crystallized with VapC (Mn^{2+}, Mg^{2+}) are shown as grey spheres.
580 (**B**) Surface conservation of the SMG5 (purple) and SMG6 (green) PIN domain interface, with
581 increasing color darkness corresponding to increased conservation.
582 (**C**) Sequence alignment of the extended SMG6 PIN domain including β1 strand and α1 helix.
583 Orthologs from *Homo sapiens* (*Hs*), *Mus musculus* (*Mm*), *Gallus gallus* (*Gg*), *Xenopus tropicalis* (*Xt*),
584 *Danio rerio* (*Dr*), *Strongylocentrotus purpuratus* (*Sp*, Purple urchin), *Drosophila melanogaster* (*Dm*)
585 and *Caenorhabditis elegans* (*Ce*) are compared, and residues with complete conservation and 70%
586 similarity are highlighted in dark and light green, respectively. Predicted secondary structure
587 elements of *Hs* and *Ce* proteins are denoted above and below the alignment, respectively. Residues
588 involved in the predicted SMG5 interface (purple), active site metal coordination (yellow) and RNA
589 substrate binding (grey) are indicated by circles above the alignment. Red stars mark amino acids
590 that were mutated in this study, while red borders mark residues that correspond to VapC active site
591 components.

592 **Figure 3. SMG5-PIN and SMG6-PIN together degrade RNA in a Mn^{2+} dependent manner.**
593 (**A**) Schematic of the gel-based *in vitro* RNA degradation assay using 5'-6FAM-conjugated RNA oligo
594 (5'-6FAM-deoxyU-U_{25}-deoxyU-3').
595 (**B**) Cleavage assay using 3 μM 5'-6FAM RNA oligo incubated with 3 μM of the indicated protein
596 constructs in 5 μL of reaction buffer (100 mM NaCl, 5 mM $MnCl_2$, 1 mM DTT, 10% glycerol, 25 mM
597 Tris-HCl pH 7.5) for 45 min (or 0 min for controls) at 37 °C. Reactions were run on 10% PAGE-Urea
598 gels. The bands corresponding to intact substrate and decay products are indicated.
599 (**C**) Quantification of RNA gel degradation assay from (C) and from three additional replicates of
600 identical experiments. The amount of remaining probe (upper band) with regard to the 0 min

601 timepoint (=100%) was quantified. Data are plotted as means ± SD. *P*-values were calculated using
602 two-tailed unpaired *t*-test.
603 (**D**) Similar to experiment shown in panel (C), 3 μM of substrate and 3 μM of indicated protein con-
604 structs were incubated with either 5 mM $MnCl_2$, $MgCl_2$, or $ZnCl_2$ in a 5 μL reaction volume (buffer
605 conditions: 100 mM NaCl, 1 mM EGTA, 1 mM DTT, 10% glycerol, 25 mM Tris-HCl pH 7.5). After
606 0 min and 45 min at 37 °C, reactions were analysed by PAGE. 30 mM EDTA (last 3 lanes) was used
607 to show the specificity of Mn^{2+}-mediated RNA degradation.
608 (**E**) Quantification of degradation assay shown in (E).

609 **Figure 4. Covalent tethering and low temperature stabilize weak SMG5-SMG6 PIN domain**
610 **interaction to enhance catalytic activity.**
611 (**A**) Cleavage assay using 3 μM 5'-6FAM RNA oligo incubated with 3 μM of the indicated protein
612 constructs in 5 μL of reaction buffer (100 mM NaCl, 5 mM $MnCl_2$, 1 mM DTT, 10% glycerol, 25 mM
613 Tris-HCl pH 7.5) for 45 min (or 0 min for controls) at 37 °C. Reactions were run on 10% PAGE-Urea
614 gels. Lanes 13 and 14 show the covalently tethered SMG5 PIN(α extension) and SMG6 PIN(α ex-
615 tension), using the SpyTag/SpyCatcher strategy.
616 (**B**) Quantification of RNA gel degradation assay from (A) and from three additional replicates of
617 identical experiments. The amount of remaining probe (upper band) with regard to the 0 min
618 timepoint (=100%) was quantified. Data are plotted as means ± SD. *P*-values were calculated using
619 two-tailed unpaired *t*-test. Note that apart from the values in lanes 13 and 14 – showing the
620 SpyTag/SpyCatcher-tethered SMG5-SMG6 pair – this graph reports on the same experimental data
621 as in Figure 3 (B) for lanes 1-12.
622 (**C**) As in (A), yet with experiments carried out at reaction temperatures of 42, 37, 10, or 0 °C.
623 (**D**) Quantification of the assay shown in (C).

624 **Figure 5. Real-time fluorescent cleavage assay reveals kinetic differences among SMG5-**
625 **SMG6 constructs.**
626 (**A**) Schematic of the real-time fluorescent cleavage assay using the 5'-6FAM-dU-U_{25}-dU-3'-BHQ1
627 substrate (termed 5'-6FAM-3'-BHQ1 in remainder of figure legends).

628 (**B**) 3 μM 5'-6FAM-3'-BHQ1 oligo were incubated with 3 μM of the indicated protein constructs (or
629 RNase-free water, as control) in 10 μL volume (reaction buffer: 100 mM NaCl, 5 mM $MnCl_2$, 1 mM
630 EGTA, 1 mM DTT, 10% glycerol, 25 mM Tris-HCl pH 7.5) for 60 min at 25 °C, with measurements at
631 1 min interval in a plate reader. Raw fluorescence values were plotted for each reaction (each con-
632 dition run in triplicates) as medians ± SD.
633 (**C**) Observed rate constants (k_{obs}) calculated from each sample shown in (B). Data are plotted as
634 means ± SD. The *P*-values were calculated using two-tailed unpaired *t*-test.

635 **Figure 6. Mutational analysis confirms composite active site and PIN-PIN interface in SMG5-**
636 **SMG6 complex.**
637 (**A**) 3 μM 5'-6FAM-3'-BHQ1 oligo were incubated with 3 μM of the indicated protein constructs that
638 probe the catalytic site residues and its environment (SMG5 D893A, K896A, K897A and SMG6
639 D1353A) in 10 μL volume (reaction buffer: 100 mM NaCl, 5 mM $MnCl_2$, 1 mM EGTA, 1 mM DTT,
640 10% glycerol, 25 mM Tris-HCl pH 7.5) for 60 min at 25 °C, with measurements at 1 min interval in a
641 plate reader. Raw fluorescence values were plotted for each reaction (each condition run in tripli-
642 cates) as averages with error bars corresponding to ± SD.
643 (**B**) Identical to (A), but for mutants that probe the interaction interface (SMG5 E910R, SMG6
644 R1396E).
645 (**C**) Observed rate constants (k_{obs}) calculated from each sample shown in (A). Data are plotted as
646 means ± SD. The *P*-values were calculated using two-tailed unpaired *t*-test.
647 (**D**) As in (C), for data shown in (B).
648 (**E**) Model of SMG5-dependent activation of SMG6 PIN nuclease through co-recruitment to
649 phosphorylated UPF1 that is bound to PTC containing mRNA.

650 **Supplementary Figures**

651 **Figure S1. Structural predictions of SMG5-6-7 complexes across evolution. Related to Figures**
652 **1, 2 and SI Figure S2.**

653 (**A**) AlphaFold3 model of the full-length *Hs*SMG5-6-7 complex with U_6 RNA and 2 Mg^{2+} (ipTM=0.41,
654 pTM=0.46). Intra- and intermolecular complexes that were predicted with high confidence (expected
655 position error ≤5Å) are highlighted in purple (extended SMG5-6PIN domains complex), blue (SMG5-
656 7 14-3-3/α-helical domains complex) and chartreuse (SMG6 14-3-3/α-helical domains).

657 (**B**) Predicted Aligned Error (PAE = expected position error) plot for the model in (A). Coloured
658 outlines mark structural domains and complexes with high predicted likelihoods corresponding to
659 (A).

660 (**C**) AlphaFold3 model of the full-length *Dm*Smg5-6 complex with U_6 RNA and 2 Mg^{2+} (ipTM=0.48,
661 pTM=0.42). Intra- and intermolecular complexes that were predicted with high confidence (PAE ≤5Å)
662 are highlighted in purple (extended SMG5-6PIN domains complex), blue (SMG5 14-3-3/α-helical
663 domains) and chartreuse (SMG6 14-3-3/α-helical domains).

664 (**D**) PAE plot for the model in (C). Coloured outlines mark structural domains and complexes with
665 high predicted likelihoods corresponding to (C).

666 (**E**) AlphaFold3 model of the full-length *Ce*SMG-5-6-7 complex with U_6 RNA and 2 Mg^{2+} (ipTM=0.37,
667 pTM=0.46).

668 (**F**) Intra- and intermolecular complexes that were predicted with high confidence (PAE ≤5Å) are
669 highlighted in purple (extended SMG5-6PIN domains complex), blue (SMG5 14-3-3/α-helical
670 domains complex) and chartreuse (SMG6 14-3-3/α-helical domains).

671 **Figure S2. Local confidence of AlphaFold3 models. Related to Figures 1, 2 and SI Figure S1.**

672 (**A**) Predicted local distance difference test (pLDDT) values per residue for the AlphaFold3 model of
673 the *Hs*SMG5-6-7 – RNA – Mg^{2+} complex. pLDDT scores from 100-0 are coloured in gradients for
674 SMG5 (from dark purple to light blue), SMG6 (from dark to light green), SMG7 (from dark orange to
675 light yellow), and RNA (from black to white). Structures are oriented as in Figure S1 (A).

676 (**B**) pLDDT values per residue for the AlphaFold3 model of the *Dm*Smg5-6 – RNA – Mg^{2+} complex.
677 pLDDT scores from 100-0 are coloured in gradients analogous to (A). Orientation of the model as in
678 Figure S1 (C).
679 (**C**) pLDDT values per residue for the AlphaFold3 model of the *Ce*SMG-5-6-7 – RNA – Mg^{2+} complex.
680 pLDDT scores from 100-0 are coloured in gradients analogous to (A). Model orientations correspond
681 to Figure S1 (E).

682 **Figure S3. Active site conservation across evolution and alignment of SMG5. Related to**
683 **Figures 1, 2, and SI Figures S1, S2.**
684 (**A**) Model of the complex between extended PIN domains of *Dm*Smg5 (purple, pink) and Smg6 (light
685 and dark green) based on the AlphaFold3 model of the full-length *Dm*Smg5-6 complex with U_6-RNA
686 and 2 Mg^{2+}. RNA (grey) and metal ions (yellow spheres) indicate the active site location, for which a
687 detailed view with active site residues shown as sticks and labelled is given below.
688 (**B**) Same as in (A) but for the model of the *Ce*SMG-5-6 PIN domain complex.
689 (**C**) Sequence alignment of the extended SMG5 PIN domain including α1 helix. Orthologs from *Homo*
690 *sapiens* (*Hs*), *Mus musculus* (*Mm*), *Gallus gallus* (*Gg*), *Xenopus tropicalis* (*Xt*), *Danio rerio* (*Dr*),
691 *Strongylocentrotus purpuratus* (*Sp*, Purple urchin), *Drosophila melanogaster* (*Dm*) and
692 *Caenorhabditis elegans* (*Ce*) are compared, and residues with complete conservation and 70%
693 similarity are highlighted in dark and light purple, respectively. Predicted secondary structure
694 elements of *Hs* and *Ce* proteins are denoted above and below the alignment, respectively. Residues
695 involved in the predicted SMG6 interface (green), active site metal coordination (yellow) and RNA
696 substrate binding (grey) are indicated by circles above the alignment. Red stars mark amino acids
697 that were mutated in this study.

698 **Figure S4. Recombinant proteins used for *in vitro* assays. Related to Figures 3-6.**
699 (**A**) Coomassie blue-stained gel showing the individual recombinant, tagged SMG5 and SMG6
700 proteins used in the study.
701 (**B**) Coomassie blue-stained gel showing the recombinant SpyTag/SpyCatcher-tethered
702 SMG5/SMG6 proteins used in the study.

703 To ensure similar staining for large and small proteins, 10 µL of a 2 µM protein solution were loaded
704 for all large proteins – i.e., for lanes 6-10 in (A) and all proteins in (B) – and 10 µL of a 10 µM protein
705 solution for smaller proteins – i.e., lanes 1-5 in (A).

706 **Figure S5. Extended mutational analysis confirms composite active site and PIN-PIN interface**
707 **in SMG5-SMG6 complex. Related to Figure 6.**

708 (**A**) As in main Figure 6C, analysis of kinetic differences between active site mutants (SMG5 D893A,
709 K896A, K897A and SMG6 D1353A), here in the SpyTag-SMG5 PIN(α-extension) / SpyCatcher-
710 SMG6 PIN(α-extension) setup.

711 (**B**) Observed rate constants (k_{obs}) calculated from each sample shown in (A). Data are plotted as
712 means ± SD. The *P*-values were calculated using two-tailed unpaired *t*-test.

713 (**C**) Related to main Figure 6E, this experiment shows the analysis of interaction surface mutant
714 SMG6 V1397E, using SMG5 PIN(α-extension) and SMG5 PIN(14-3-3-extension) setup.

715 (**D**) Observed rate constants (k_{obs}) calculated from data in (B). Data are plotted as means ± SD. The
716 *P*-values were calculated using two-tailed unpaired *t*-test.

717 (**E**) Similar experiment as in (C), probing the interaction surface mutant SMG6 V1397E, but in the
718 SpyTag-SMG5 PIN(α-extension) / SpyCatcher-SMG6 PIN(α-extension) setup.

719 (**F**) Observed rate constants (k_{obs}) calculated from data in (E). Data are plotted as means ± SD. The
720 *P*-values were calculated using two-tailed unpaired *t*-test.

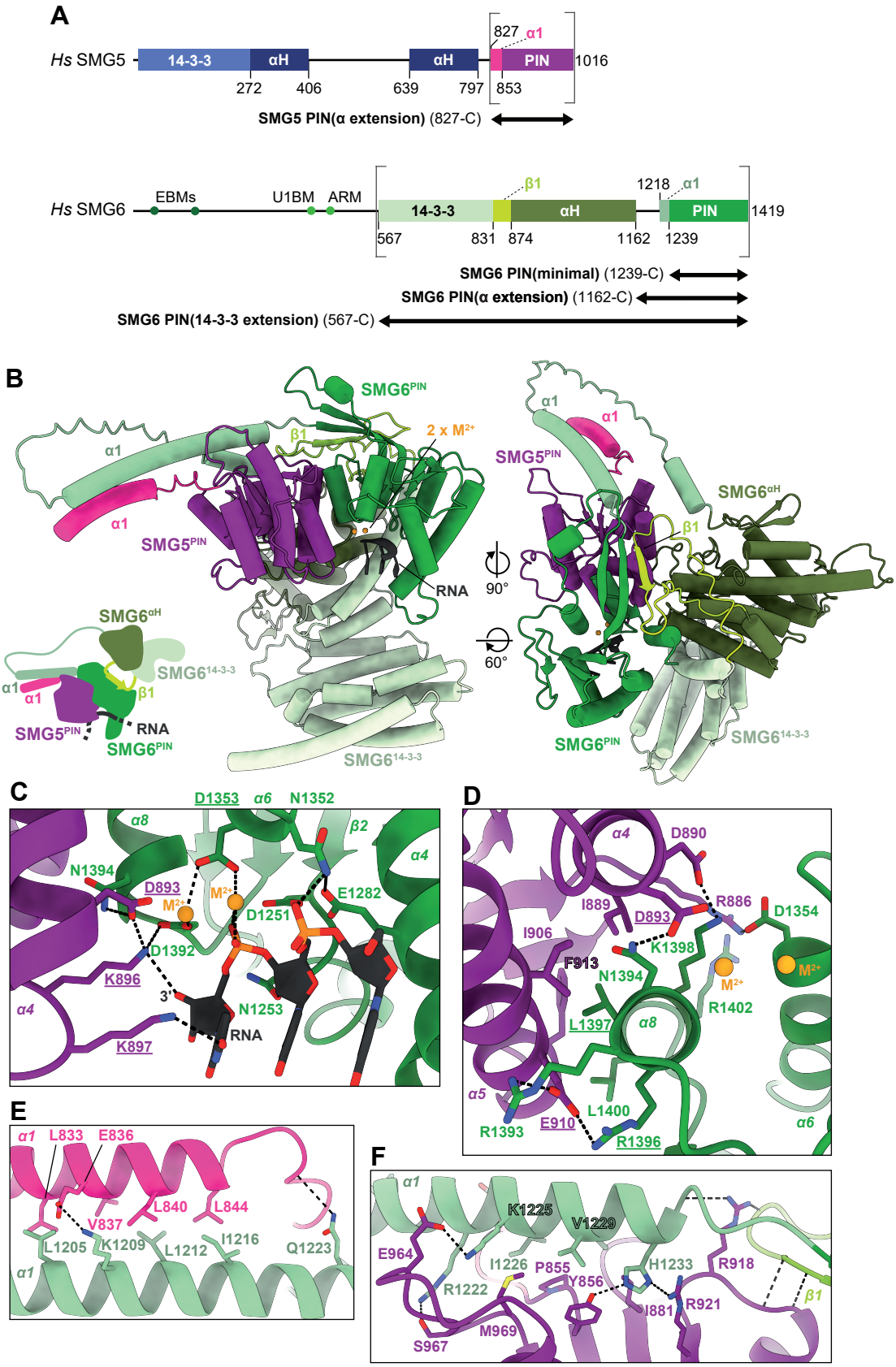
A
Hs SMG5
14-3-3
αH
αH
PIN
827
α1
1016
272
406
639
797
853
SMG5 PIN(α extension) (827-C)
Hs SMG6
EBMs
U1BM
ARM
14-3-3
β1
αH
1218
α1
PIN
1419
567
831
874
1162
1239
SMG6 PIN(minimal) (1239-C)
SMG6 PIN(α extension) (1162-C)
SMG6 PIN(14-3-3 extension) (567-C)
B
SMG6PIN
2 x M2+
α1
β1
SMG5PIN
RNA
SMG6αH
SMG6 14-3-3
SMG6PIN
90°
60°
C
D1353
α6
N1352
α8
β2
α4
N1394
D893
M2+
E1282
D1251
D1392
K896
3'
N1253
RNA
K897
D
D890
I889
R886
D1354
I906
K1398
F913
N1394
R1402
L1397
α8
α5
L1400
R1393
E910
R1396
α6
E
L833
E836
L840
L844
V837
L1205
K1209
L1212
I1216
Q1223
F
K1225
V1229
E964
I1226
P855
Y856
H1233
R918
R1222
I881
R921
M969
S967
β1

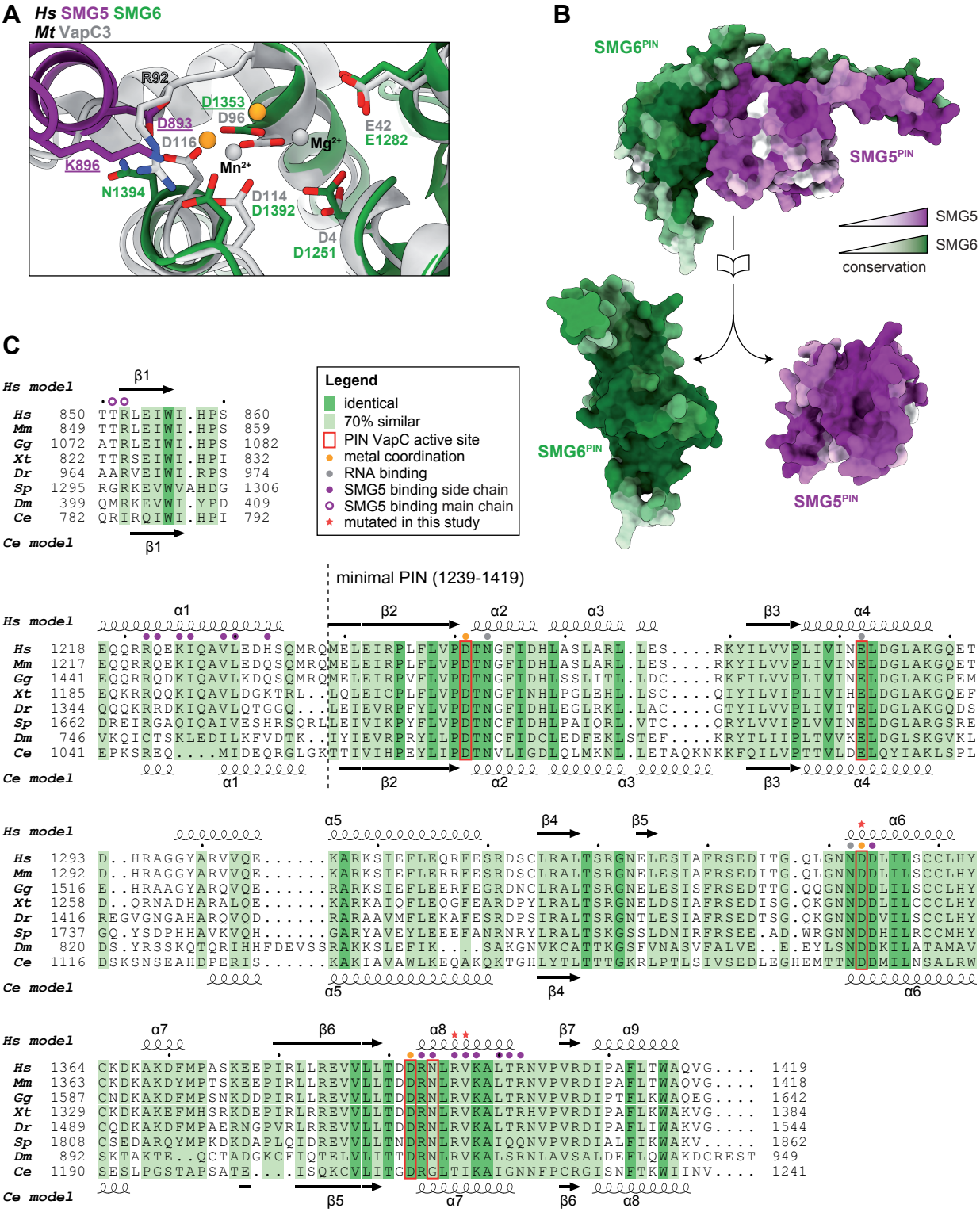
A
Hs SMG5 SMG6
Mt VapC3
R92
D1353
D96
D893
D116
Mg2+
E42
E1282
K896
Mn2+
N1394
D114
D1392
D4
D1251
B
SMG6PIN
SMG5PIN
SMG5
SMG6
conservation
SMG6PIN
SMG5PIN
C
Hs model
β1
Hs 850 TTRLEIWI.HPS 860
Mm 849 TTRLEIWI.HPS 859
Gg 1072 ATRLEIWI.HPS 1082
Xt 822 TTRSEIWI.HPI 832
Dr 964 AARVEIWI.RPS 974
Sp 1295 RGRKEVWVAHDG 1306
Dm 399 QMRKEVWI.YPD 409
Ce 782 QRIRQIWI.HPI 792
Ce model
β1
Legend
identical
70% similar
PIN VapC active site
metal coordination
RNA binding
SMG5 binding side chain
SMG5 binding main chain
mutated in this study
minimal PIN (1239-1419)
Hs model
α1 β2 α2 α3 β3 α4
Hs 1218 EQQRRQEKIQAVLEDHSQMRQMELEIRPLFLVPDTNGFIDHLASLARL.LES....RKYILVVPLIVINELDGLAKGQET
Mm 1217 EQQRRQEKIQAVLEDQSQMRQMELEIRPLFLVPDTNGFIDHLASLARL.LES....RKYILVVPLIVINELDGLAKGQET
Gg 1441 EQQRRQDKIQAVLKDQSQMRQMELEIRPVFLVPDTNGFIDHLSSLITL.LDC....RKFILVVPLIVINELDGLAKGPEM
Xt 1185 EQKRRQQKIQAVLDGKTRL..LQLEICPLFLVPDTNGFINHLPGLEHL.LSC....QIYILVIPLIVIHELDGLAKGQEF
Dr 1344 QQQKRRDKIQAVLQTGGQ...LEIEVRPFYLVPDTNGFIDHLEGLRKL.LAC....GTYILVVPLIVITELDGLAKGQDS
Sp 1662 DREIRGAQIQAIVESHRSQRLLEIVIKPYFLVPDTNCFIDHLPAIQRL.VTC....QRYLVVIPLVVINELDGLARGSRE
Dm 746 VKQICTSKLEDILKFVDTK..IYIEVRPRYLLPDTNCFIDCLEDFEKLSTEF....KRYTLIIPLTVVKELDGLSKGVKL
Ce 1041 EPKSREQ....MIDEQRGLGKTTIVIHPEYLIPDTNVLIGDLQLMKNL.LETAQKNKKFQILVPTTVLDELQYIAKLSPL
Ce model
α1 β2 α2 α3 β3 α4
Hs model
α5 β4 β5 α6
Hs 1293 D..HRAGGYARVVQE.....KARKSIEFLEQRFESRDSCLRALTSRGNELESIAFRSEDITG.QLGNNDDLILSCCLHY
Mm 1292 D..HRAGGYARVVQE.....KARKSIEFLERRFESRDSCLRALTSRGNELESIAFRSEDITG.QLGNNDDLILSCCLHY
Gg 1516 E..HRAAGYARQVQE.....RARKSIEFLEERFEGRDNCLRALTSRGNELESISFRSEDTTG.QQGNNDDLILSCCLHY
Xt 1258 D..QRNADHARALQE.....KARKAIQFLEQGFEARDPYLRALTSRGNELDSIAFRSEDISG.QKGNNDDLILCCCLHY
Dr 1416 REGVGNGAHARQVQD.....RARAAVMFLEKAFESRDPSIRALTSRGNTLESIAFRSEDTSG.QKGNNDDVILSCCLHY
Sp 1737 GQ.YSDPHHAVKVQH.....GARYAVEYLEEEFANRNRYLRALTSKGSSLDNIRFRSEE.AD.WRGNNDDHILRCCMHY
Dm 820 DS.YRSSKQTQRIHHFDEVSSRAKKSLEFIK....SAKGNVKCATTKGSFVNASVFALVE..E.EYLSNDDKILATAMAV
Ce 1116 DSKSNSEAHDPERIS.....KAKIAVAWLKEQAKQKTGHLYTLTTTGKRLPTLSIVSEDLEGHEMTTNDDMILNSALRW
Ce model
α5 β4 α6
Hs model
α7 β6 α8 β7 α9
Hs 1364 CKDKAKDFMPASKEEPIRLLREVVLLTDDRNLRVKALTRNVPVRDIPAFLTWAQVG.... 1419
Mm 1363 CKDKAKDYMPTSKEEPIRLLREVVLLTDDRNLRVKALTRNVPVRDIPAFLTWAQVG.... 1418
Gg 1587 CNDKAKDFMPSNKDDPIRLLREVVLLTDDRNLRVKALTRNVPVRDIPTFLKWAQEG.... 1642
Xt 1329 CKDKAKEFMHSRKDEPIRLRREVVLLTDDRNLRVKALTRHVPVRDIPAFLKWAKVG.... 1384
Dr 1489 CQDKAKDFMPAERNGPVRLRREVVLLTDDRNLRVKALTRNVPVRDIPAFLIWAKVG.... 1544
Sp 1808 CSEDARQYMPKDKDAPLQIDREVVLLTNDRNLRVKAIQQNVPVRDIALFIKWAKV..... 1862
Dm 892 SKTAKTE..QCTADGKCFIQTELVLITTDRNLRVKALSRNLAVSALDEFLQWAKDCREST 949
Ce 1190 SESLPGSTAPSATE....ISQKCVLITGDRGLTIKAIGNNFPCRGISNFTKWIINV.... 1241
Ce model
β5 α7 β6 α8 β7 α9

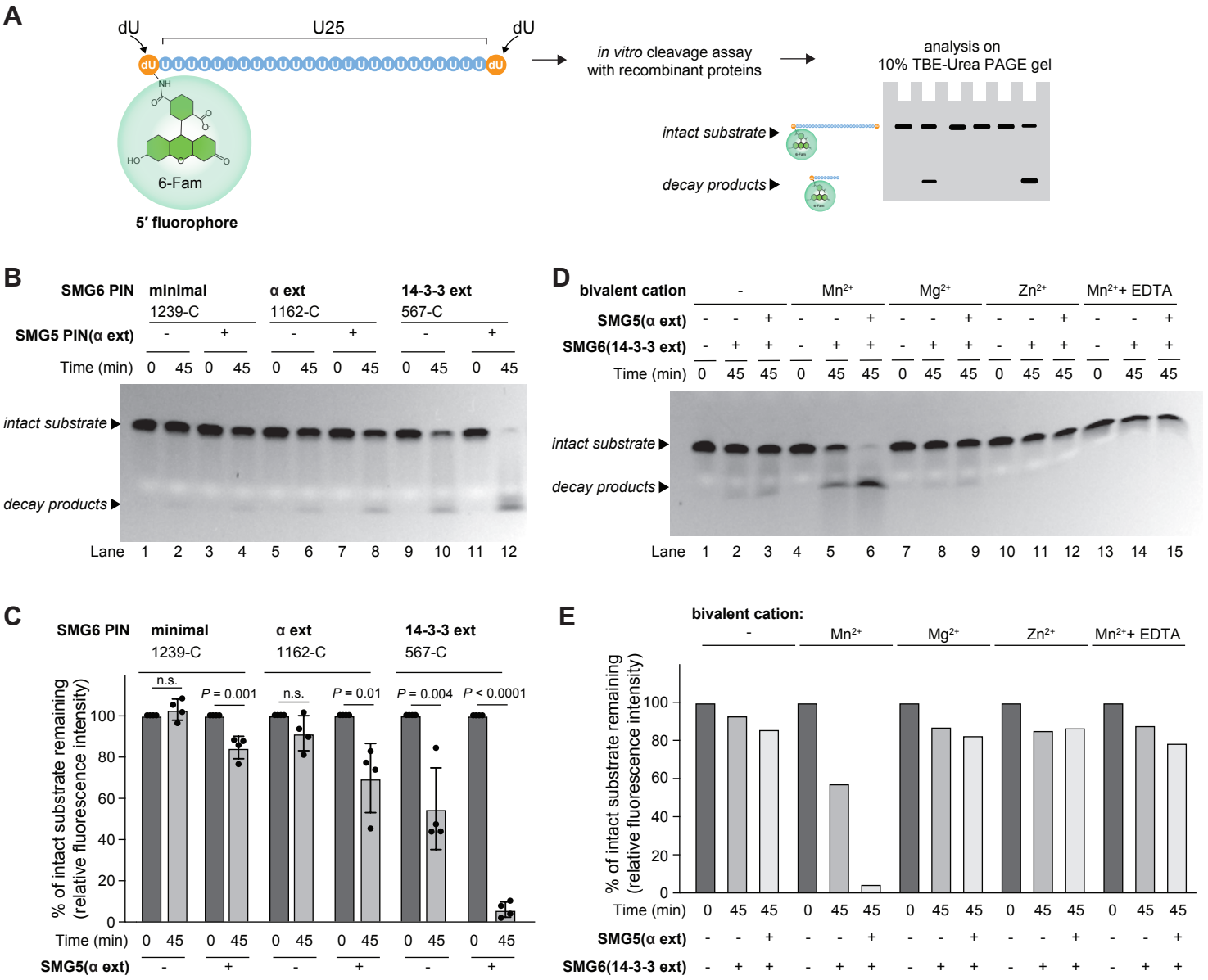
A
dU
U25
dU
6-Fam
5′ fluorophore
in vitro cleavage assay
with recombinant proteins
analysis on
10% TBE-Urea PAGE gel
intact substrate
decay products
B
SMG6 PIN
minimal
1239-C
α ext
1162-C
14-3-3 ext
567-C
SMG5 PIN(α ext)
Time (min)
intact substrate
decay products
Lane
D
bivalent cation
Mn2+
Mg2+
Zn2+
Mn2+ + EDTA
SMG5(α ext)
SMG6(14-3-3 ext)
Time (min)
intact substrate
decay products
Lane
C
SMG6 PIN
minimal
1239-C
α ext
1162-C
14-3-3 ext
567-C
n.s.
P = 0.001
n.s.
P = 0.01
P = 0.004
P < 0.0001
% of intact substrate remaining
(relative fluorescence intensity)
Time (min)
SMG5(α ext)
E
bivalent cation:
Mn2+
Mg2+
Zn2+
Mn2+ + EDTA
% of intact substrate remaining
(relative fluorescence intensity)
Time (min)
SMG5(α ext)
SMG6(14-3-3 ext)

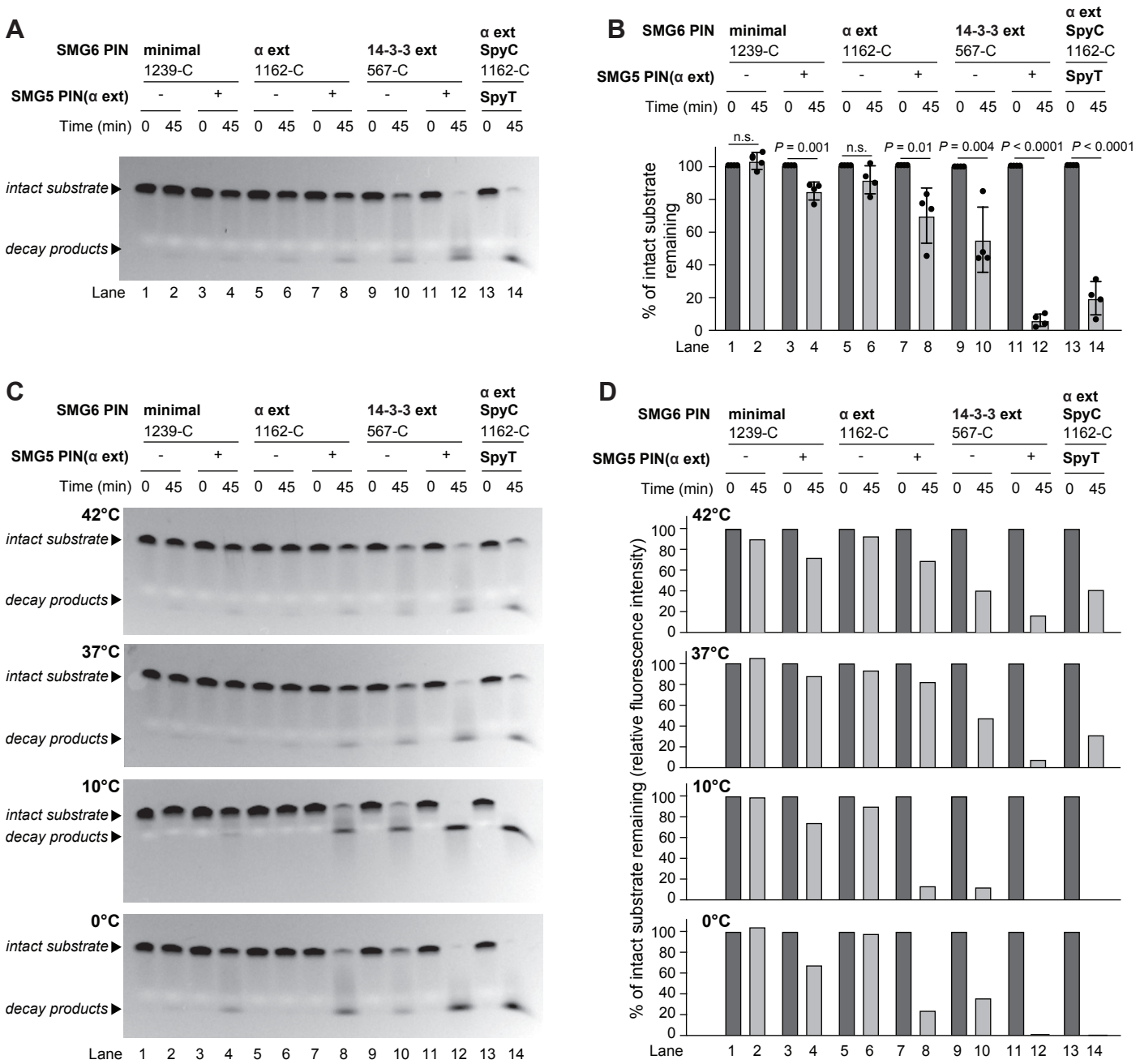
A
SMG6 PIN
minimal
1239-C
α ext
1162-C
14-3-3 ext
567-C
α ext
SpyC
1162-C
SMG5 PIN(α ext)
-
+
SpyT
Time (min)
0 45
intact substrate
decay products
Lane 1 2 3 4 5 6 7 8 9 10 11 12 13 14
B
% of intact substrate remaining
n.s.
P = 0.001
P = 0.01
P = 0.004
P < 0.0001
P < 0.0001
C
42°C
37°C
10°C
0°C
D
% of intact substrate remaining (relative fluorescence intensity)

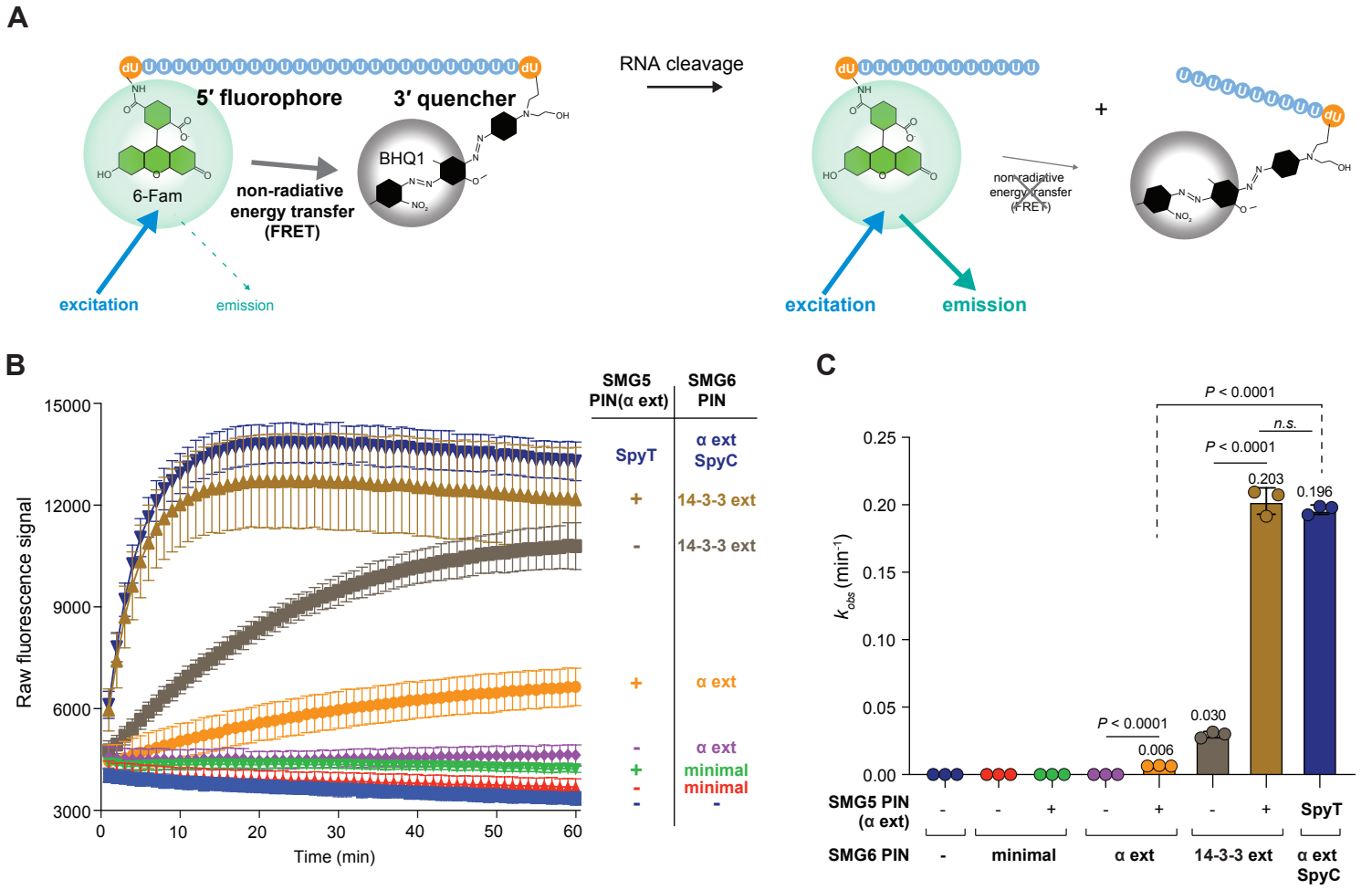
A
5′ fluorophore
3′ quencher
6-Fam
BHQ1
non-radiative energy transfer (FRET)
excitation
emission
RNA cleavage
B
Raw fluorescence signal
Time (min)
SMG5 PIN(α ext)
SMG6 PIN
SpyT
α ext SpyC
+
14-3-3 ext
-
14-3-3 ext
+
α ext
-
α ext
+
minimal
-
minimal
-
-
C
k_{obs} (min^{-1})
P < 0.0001
n.s.
P < 0.0001
0.203
0.196
P < 0.0001
0.030
0.006
SMG5 PIN (α ext)
SMG6 PIN
minimal
α ext
14-3-3 ext
α ext SpyC
SpyT

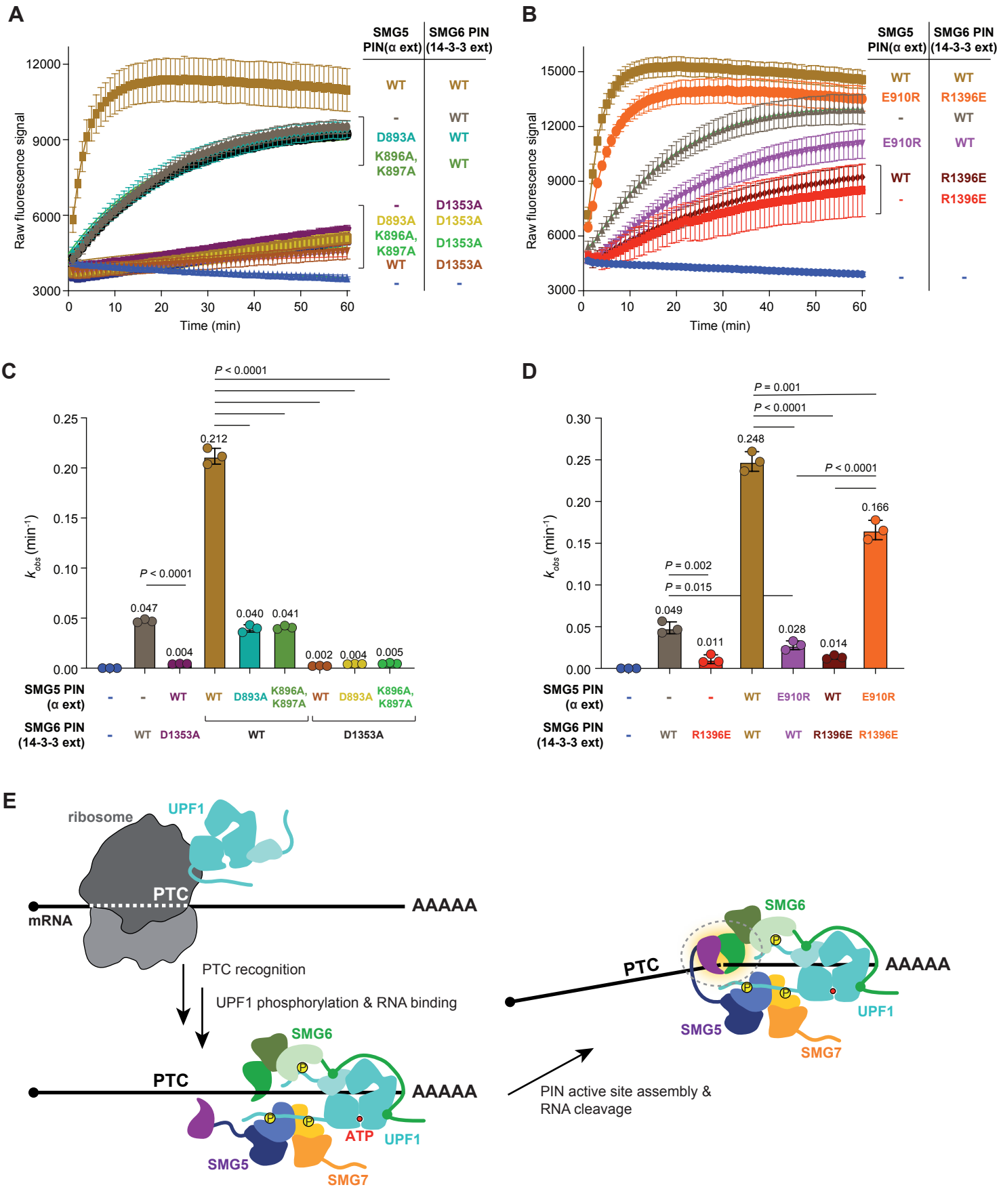
A
SMG5 PIN(α ext)
SMG6 PIN (14-3-3 ext)
Raw fluorescence signal
Time (min)
WT
WT
-
WT
D893A
WT
K896A, K897A
WT
-
D1353A
D893A
D1353A
K896A, K897A
D1353A
WT
D1353A
-
-
B
SMG5 PIN(α ext)
SMG6 PIN (14-3-3 ext)
Raw fluorescence signal
Time (min)
WT
WT
E910R
R1396E
-
WT
E910R
WT
WT
R1396E
-
R1396E
-
-
C
P < 0.0001
P < 0.0001
k_{obs} (min^{-1})
0.047
0.004
0.212
0.040
0.041
0.002
0.004
0.005
SMG5 PIN (α ext)
SMG6 PIN (14-3-3 ext)
WT
D1353A
WT
D1353A
D893A
K896A, K897A
D893A
K896A, K897A
D
P = 0.001
P < 0.0001
P = 0.002
P = 0.015
P < 0.0001
k_{obs} (min^{-1})
0.049
0.011
0.248
0.028
0.014
0.166
SMG5 PIN (α ext)
SMG6 PIN (14-3-3 ext)
WT
R1396E
WT
WT
R1396E
R1396E
E910R
E910R
E
ribosome
UPF1
PTC
mRNA
AAAAA
PTC recognition
UPF1 phosphorylation & RNA binding
SMG6
PTC
AAAAA
ATP
UPF1
SMG5
SMG7
PIN active site assembly & RNA cleavage
SMG6
PTC
AAAAA
UPF1
SMG5
SMG7